JOURNAL OF THERMOPHYSICS AND HEAT TRANSFER
Vol. 23, No. 3, July–September 2009

Analytical and Kinetic Modeling of Ablation Process

L. Pekker,* N. Gimelshein,† and S. Gimelshein‡
ERC, Inc., Edwards Air Force Base, California 93524

DOI: 10.2514/1.41309

One of the most important issues in the computation fluid dynamics modeling of the ablation process is the formulation of boundary conditions at the gas–surface interface. These boundary conditions cannot be obtained without analytical or parametric numerical modeling of the Knudsen layer formed near the evaporating surface. Analytical models are therefore of interest for the numerical simulation of ablating flows. The recently developed Pekker–Keidar–Cambier model of the Knudsen layer takes into account the temperature gradient in the bulk gas. This model uses a bimodal velocity distribution function that preserves the laws of conservation of mass, momentum, and energy within the Knudsen layer and converges to the Chapman–Enskog velocity distribution function at the outer boundary of the Knudsen layer. The main objective of this work is to provide detailed analysis of the applicability of this analytical model by comparing its predictions with the numerical solutions of the ellipsoidal statistical Bhatnagar–Gross–Krook model kinetic equation and the results obtained with the direct simulation Monte Carlo method.

Nomenclature

A	=	plate A
B	=	plate B
bulk	=	gas bulk region
E_x	=	energy flux
eq	=	equilibrium
i	=	plate A or B
k	=	Boltzmann constant
L	=	distance between the plates
M_x	=	mass flux
m	=	mass of a vapor molecule
n	=	number density
P_x	=	momentum flux
T	=	temperature
u	=	directed gas velocity
V_T	=	thermal velocity
x	=	axis directed from plate A to B
x_i	=	ratio of the directed gas velocity to the thermal velocity at the outer boundary of the ith Knudsen layer
β	=	parameter of the gas velocity distribution function in the Knudsen layer
δx_T	=	characteristic temperature gradient length
λ_{mfp}	=	mean free path
τ_T	=	thermal conduction parameter
χ_{gas}	=	thermal conductivity of the bulk gas
$*$	=	index for intermediate values calculated by the iterative algorithm

I. Introduction

THE first analytical model of the Knudsen layer at an ablating surface was introduced by Hertz [1] and Knudsen [2]. It assumes no collisions in the Knudsen layer, no heat transfer in the bulk gas, and the complete absorption of all incoming molecules at the wall, which corresponds to the condensation coefficient of 1. The condensation coefficient is defined as the ratio of incident molecules absorbed by the surface to those colliding with the surface. This classical model, along with its generalizations, has been widely used in the computational fluid dynamics (CFD) modeling of the ablation process [3,4]. In their recent paper, Bond and Struchtrup [5] have extended the Hertz–Knudsen model to the case of thermal conduction in the bulk gas, considered diffuse and specular reflections of particles, and allowed for nonflat wall–gas interfaces. However, their model still ignores collisions in the Knudsen layer, which means that the momentum conservation does not hold there. It should be noted that the Hertz–Knudsen assumption of no collisions in the Knudsen layer is not self-consistent, because it assumes no relaxation in the kinetic (Knudsen) layer, even though the velocity distribution function at the ablative surface has to relax to the gas bulk (equilibrium) distribution function in the Knudsen layer.

Anisimov [6] was the first to introduce a bimodal velocity distribution function in the Knudsen layer when studding the vaporization of a metal surface exposed to laser ablation. In this model, Anisimov used mass, momentum, and energy conservation laws to determine the parameters of his bimodal velocity distribution function, thus accounting for collisions in the Knudsen layer. The assumptions in his model are as follows:

1) The flow velocity at the outer boundary of the Knudsen layer is equal to the speed of sound.

2) The gas temperature in the equilibrium (bulk gas) region outside the Knudsen layer (see Fig. 1) is constant, that is, there is no conductive heat flux to the ablative surface.

3) All particles that hit the ablative surface are absorbed by it.

Since then, the Anisimov method has been extended to the half-space evaporation problem [7] and evaporation into dense plasma [8–12], for which the flow velocity at the outer boundary of the Knudsen layer was assumed to be smaller than the speed of sound and dependent on the properties of the bulk gas. In all these models, the authors still assume no conductive heat flux to the ablative surface and complete absorption of particles by the ablative surface. However, the temperature in the plasma core [8–12] is much higher than the temperature of the ablative surface; therefore, the thermal conduction can be significant and has to be included in a Knudsen layer model. Pekker et al. [13] used a new bimodal velocity distribution function in the kinetic layer and built a more general Knudsen layer model that takes into account the conductivity of the bulk gas and can therefore be used to simulate flows with large temperature gradients. Their bimodal velocity distribution function in the Knudsen layer preserves the laws of conservation of mass, momentum, and energy and converges to the Chapman–Enskog velocity distribution function at the outer boundary of the layer. However, as

Presented as Paper 3803 at the 40th Thermophysics Conference, Seattle, WA, 23–26 June 2008; received 29 September 2008; revision received 2 February 2009; accepted for publication 15 February 2009.

*Research Scientist, 10 East Saturn Boulevard; leonid.pekker.ctr@edwards.af.mil.

†Consultant, 10 East Saturn Boulevard; ngimel@gmail.com.

‡Consultant, 10 East Saturn Boulevard; gimelshe@usc.edu.

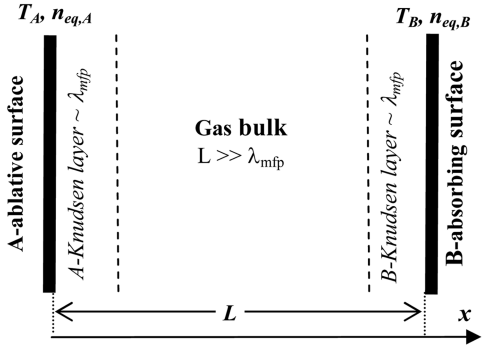

Fig. 1 Schematic representation of the model

with all other bimodal velocity distribution function models, the condensation coefficient of the model [13] was assumed to be equal to unity. Then Pekker [14] extended the model [13] to the case of an arbitrary condensation coefficient. He also assumed a constant accommodation coefficient that specifies the fractions of diffuse and specular collisions of incident particles on the ablative surface. This model allowed the author to formulate gas–surface boundary conditions that can be used for CFD modeling of ablation processes, which takes into account thermal conduction and incorporates arbitrary condensation and accommodation coefficients.

The ablation process can generally be modeled using the Boltzmann equation for the gas near the ablative surface with the boundary conditions at the surface. The latter describe the fluxes of particles that are 1) absorbed by the surface (condensation process), 2) rebounded off the surface back into the gas region (rebounding process), and 3) evaporated from the surface (evaporation process). Therefore, this process can be modeled using different methods developed for the solution of this equation, such as the direct simulation Monte Carlo (DSMC) method [15–18]. When the derivation from equilibrium is expected to be small, ablation can also be described by a Bhatnagar–Gross–Krook (BGK) kinetic model equation or by the more advanced ellipsoidal statistical BGK (ES–BGK) model [19–21]. No approximation for the gas velocity distribution function in the Knudsen layer is necessary for kinetic modeling. Even though ES–BGK solutions are usually associated with a lower computational cost for modeling low-speed flows than the DSMC method, both these methods require significant computational time, which limits their application. The authors [7,10,16–18,22] have demonstrated that the models that use a bimodal velocity distribution function [6] are in good agreement with the DSMC simulations and numerical solutions of the BGK equation for the evaporation of a monatomic substance with a condensation coefficient equal to unity. However, a thorough verification of the new analytical models of the Knudsen layer [13,14] using a detailed comparison with kinetic approaches is needed.

The main objective of this work is to provide a detailed analysis of the applicability of the Knudsen layer model [13] using a comparison of its predictions with the ES–BGK and DSMC results. To verify the model [13], we consider a one-dimensional evaporation/condensation process between two parallel plates for different Knudsen numbers. The analytical model of the evaporation process between ablative and absorbing plates, Fig. 1, including the Knudsen layer model [13], is described in Sec. II. The details of the ES–BGK and DSMC methods are given in Sec. III. Numerical results and analysis are presented in Sec. IV and the conclusions in Sec. V.

II. Analytical Model

A. Knudsen Layer

Figure 1 shows a schematic representation of the problem, where T_A and T_B are the temperatures of the A-ablative and B-absorbing surfaces, $n_{\mathrm{eq},A}$ and $n_{\mathrm{eq},B}$ are the equilibrium vapor densities of A and B wall materials at temperatures T_A and T_B, respectively, and L is the distance between the plates. For the sake of simplicity, the condensation coefficient at both surfaces is taken to be unity, thus assuming that all particles that hit the ablative surface are absorbed by it.

It should be emphasized that the temperatures of the wall surfaces, the equilibrium vapor pressures, the molecular mass of vapor molecules, and the thermal conductivity of the bulk vapor gas are the input parameters of the model. Their values are arbitrary chosen here only to illustrate the methods and verify the applicability of the analytical Knudsen layer model [13]. Thus, they will not correspond to an actual vaporization process, wall materials, etc.; however, the model certainly can be used for modeling real vaporization processes.

The equations describing the Knudsen layer [13] are

$$\frac{1}{2\cdot\sqrt{\pi}}=\left(\frac{n_{\mathrm{bulk},i}}{n_{\mathrm{eq},i}}\right)\cdot\left(\frac{V_{T_{\mathrm{bulk},i}}}{V_{T_i}}\right)\cdot\left[x_i-\frac{\beta_i}{2}\cdot\left[x_i\cdot\mathrm{erfc}(x_i)-\frac{1}{\sqrt{\pi}}\exp(-x_i^2)\right]\right] \tag{1}$$

$$\frac{1}{4}=\left(\frac{n_{\mathrm{bulk},i}}{n_{\mathrm{eq},i}}\right)\cdot\left(\frac{V_{T_{\mathrm{bulk},i}}}{V_{T_i}}\right)^2\cdot\left[\left(x_i^2+\frac{1}{2}\right)-\frac{\beta_i}{2}\cdot\left[\left(x_i^2+\frac{1}{2}\right)\cdot\mathrm{erfc}(x_i)-\frac{x_i}{\sqrt{\pi}}\cdot\exp(-x_i^2)\right]\right] \tag{2}$$

$$\frac{1}{\sqrt{\pi}}=\left(\frac{n_{\mathrm{bulk},i}}{n_{\mathrm{eq},i}}\right)\cdot\left(\frac{V_{T_{\mathrm{bulk},i}}}{V_{T_i}}\right)^3\cdot\left[x_i\cdot\left(x_i^2+\frac{5}{2}\right)-\frac{5\cdot\tau_{T_i}}{4}+\frac{\beta_i}{2}\cdot\left[\frac{1}{\sqrt{\pi}}\cdot(x_i^2+2)\cdot\exp(-x_i^2)-x_i\cdot\left(\frac{5}{2}+x_i^2\right)\cdot\mathrm{erfc}(x_i)\right]\right] \tag{3}$$

where

$$x_i=\frac{u_i}{V_{T_{\mathrm{bulk},i}}} \tag{4}$$

$$V_{T_i}=\sqrt{\frac{2\cdot k\cdot T_i}{m}},\qquad V_{T_{\mathrm{bulk},i}}=\sqrt{\frac{2\cdot k\cdot T_{\mathrm{bulk},i}}{m}} \tag{5}$$

Here, index i denotes either surface A or surface B (see Fig. 1); $V_{T_{\mathrm{bulk},i}}$, $n_{\mathrm{bulk},i}$, and u_i are the thermal velocity, number density, and directed vapor velocity at the outer boundary of the ith Knudsen layer (see Fig. 2); V_{T_i} is the thermal velocity of vapor corresponding to the wall temperature T_i; m is the mass of a vapor molecule; and x_i is the ratio of directed vapor velocity to the thermal vapor velocity at the outer boundary of the ith Knudsen layer. Equations (1–3) correspond to the laws of mass, momentum, and energy conservation inside the Knudsen layer [13], respectively. In Eq. (3), τ_{T_i} is a thermal conduction parameter:

$$\tau_{T_i}=\frac{8\cdot\chi_{\mathrm{gas}}}{5\cdot n_{\mathrm{bulk},i}\cdot k\cdot V_{T_{\mathrm{bulk},i}}^2}\cdot\left.\frac{\mathrm{d}V_{T_{\mathrm{bulk},i}}}{\mathrm{d}x}\right|_{\mathrm{KL}}=\frac{\lambda_{\mathrm{mfp},i}}{\delta x_{T,i}}\ll 1 \tag{6}$$

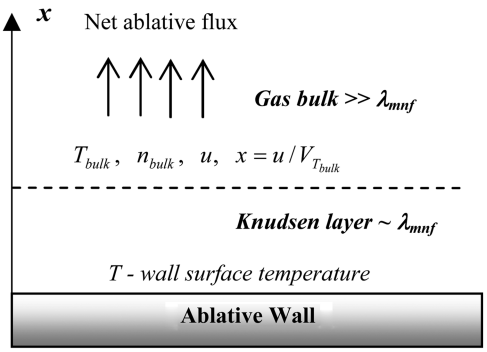

Fig. 2 Schematic representation of the layer structure near the ablative surface.

where

$$\lambda_{\mathrm{mfp},i} = \frac{4 \cdot \chi_{\mathrm{gas}}}{5 \cdot n_{\mathrm{bulk},i} \cdot k \cdot V_{T_{\mathrm{bulk},i}}} \tag{7}$$

$$\delta x_{T,i} = \frac{1}{T_{\mathrm{bulk},i}} \cdot \frac{d(T_{\mathrm{bulk},i})}{dx}\bigg|_{\mathrm{KL}} \tag{8}$$

are the gas mean free path and characteristic temperature gradient length at the outer boundary of the kinetic layer, respectively, and χ_{gas} is the thermal conductivity of the bulk gas. Condition (6), $\lambda_{\mathrm{mfp}} \ll \delta x_T$, is needed for the Chapman–Enskog expansion method to be valid [23] and is used in the derivation of Eq. (3), as shown in [13]. Parameter β in Eqs. (1–3) is an unknown that must be calculated; essentially, it represents nonequilibrium effects caused by collisions in the Knudsen layer [6]. It is worth noting that the case of $u > 0$ corresponds to the ablation process, Fig. 2, whereas the case of $u < 0$ corresponds to the absorption process.

Thus, if we know two parameters, for example x_A and τ_{T_A}, the system of Eqs. (1–3) is complete (the wall temperature T_A and equilibrium vapor number density $n_{\mathrm{eq},A}$ are assumed to be known, as they are the input parameters of the model) and $V_{T_{\mathrm{bulk},A}}$, $n_{\mathrm{bulk},A}$, and β can be calculated. Then, $T_{\mathrm{bulk},A}$ and u_A may be calculated from Eqs. (5) and (6).

B. Gas Bulk

Consider now the gas bulk region. In this region (Fig. 1), the mass flux, momentum flux, and energy flux equations [23] are

$$M_x = m \cdot n_{\mathrm{bulk}} \cdot u_{\mathrm{bulk}} \tag{9}$$

$$P_x = m \cdot n_{\mathrm{bulk}} \cdot \left(u_{\mathrm{bulk}}^2 + \frac{V_{T_{\mathrm{bulk}}}^2}{2}\right) \tag{10}$$

$$E_x = -\chi_{\mathrm{gas}} \cdot \frac{\mathrm{d}T_{\mathrm{bulk}}(z)}{\mathrm{d}z} + m \cdot n_{\mathrm{bulk}} \cdot u_{\mathrm{bulk}} \cdot \left[\frac{5}{4} \cdot V_{T_{\mathrm{bulk}}}^2 + \frac{u_{\mathrm{bulk}}^2}{2}\right] \tag{11}$$

where

$$T_{\mathrm{bulk}} = \frac{m \cdot V_{T_{\mathrm{bulk}}}^2}{2 \cdot k} \tag{12}$$

is the gas bulk temperature, and χ_{gas} is the thermal conductivity of the bulk gas. Obviously, the gas bulk density, n_{bulk}, the bulk gas temperature, T_{bulk}, and the bulk gas directed velocity, u_{bulk}, are dependent on the x coordinate (Fig. 1). In a stationary case, considered in this paper, the mass, momentum, and energy fluxes M_x, P_x, and E_x are conserved inside the bulk gas region. The boundary conditions at the outer boundaries of the A- and B-Knudsen layers can be written as

$$\begin{aligned} n_{\mathrm{bulk}}(x=0) &= n_{\mathrm{bulk},A}, \qquad V_{T_{\mathrm{bulk}}}(x=0) = V_{T_{\mathrm{bulk}},A} \\ u_{\mathrm{bulk}}(x=0) &= u_{\mathrm{bulk},A} \end{aligned} \tag{13}$$

$$\begin{aligned} n_{\mathrm{bulk}}(x=L) &= n_{\mathrm{bulk},B}, \qquad V_{T_{\mathrm{bulk}}}(x=L) = V_{T_{\mathrm{bulk}},B} \\ u_{\mathrm{bulk}}(x=L) &= u_{\mathrm{bulk},B} \end{aligned} \tag{14}$$

It is worth noting that, because the velocity distribution function in the Knudsen layer [13] converges to the Chapman–Enskog velocity distribution function at the outer boundary of the Knudsen layer, the boundary conditions (13) and (14) automatically preserve the fluxes of mass, momentum, and energy within the entire region between the two walls, including both Knudsen layers.

Expressing u_{bulk}, T_{bulk}, and n_{bulk} via $V_{T_{\mathrm{bulk}}}$, E_x, M_x, and P_x, Eqs. (9–13), we obtain

$$E_x = M_x \cdot \left(\frac{1}{2} \cdot \left[\frac{V_{T_{\mathrm{bulk}}}^2 \cdot M_x}{P_x + \sqrt{P_x^2 - 2 \cdot V_{T_{\mathrm{bulk}}}^2 \cdot M_x^2}}\right]^2 + \frac{5}{4} \cdot V_{T_{\mathrm{bulk}}}^2\right) - \frac{\chi_{\mathrm{gas}} \cdot m}{k} \cdot V_{T_{\mathrm{bulk}}} \cdot \frac{dV_{T_{\mathrm{bulk}}}}{dz} \tag{15}$$

$$u_{\mathrm{bulk}} = \frac{V_{T_{\mathrm{bulk}}}^2 \cdot M_x}{P_x + \sqrt{P_x^2 - 2 \cdot V_{T_{\mathrm{bulk}}}^2 \cdot M_x^2}} \tag{16}$$

$$n_{\mathrm{bulk}} = \frac{P_x + \sqrt{P_x^2 - 2 \cdot V_{T_{\mathrm{bulk}}}^2 \cdot M_x^2}}{m \cdot V_{T_{\mathrm{bulk}}}^2} \tag{17}$$

Thus, by numerically solving Eq. (15) for $V_{T_{\mathrm{bulk}}}$ for given E_x, M_x, and P_x, one can calculate the gas thermal velocity as a function of the x coordinate in the gas bulk region, then, using Eqs. (12), (16), and (17), obtain the distributions of T_{bulk}, u_{bulk}, and n_{bulk}, and finally calculate the thermal conduction parameter τ_T, Eq. (6), at the outer boundary of the Knudsen layer.

C. Algorithm

Let us now describe the algorithm for the calculation of the gas bulk profiles and the parameters of the Knudsen layers for given wall surfaces temperatures and corresponding equilibrium vapor number densities.

1) Assume initial values of x_A and τ_{T_A}.

2) Calculate all parameters of the A-Knudsen layer as described in the last paragraph of Sec. II.A.

3) Use Eqs. (9–11) to calculate the mass, momentum, and energy fluxes at the outer boundary of the Knudsen layer, where the temperature gradient can be determined from Eqs. (6–8).

4) Integrate Eq. (15) to obtain $V_{T_{\mathrm{bulk},B}}$, the gas thermal velocity at the outer boundary of the B-Knudsen layer. A standard first-order explicit schema was used to solve this equation:

$$\frac{V_{T_{\mathrm{bulk}}}^{z+h} - V_{T_{\mathrm{bulk}}}}{h} = \left\{\left[E_x - M_x \cdot \left(\frac{1}{2} \cdot \left[\frac{V_{T_{\mathrm{bulk}}}^2 \cdot M_x}{P_x + \sqrt{P_x^2 - 2 \cdot V_{T_{\mathrm{bulk}}}^2 \cdot M_x^2}}\right]^2 + \frac{5}{4} \cdot V_{T_{\mathrm{bulk}}}^2\right)\right] \cdot \frac{k}{\chi_{\mathrm{gas}} \cdot m \cdot V_{T_{\mathrm{bulk}}}}\right\}^z$$

5) Use Eqs. (16), (17), and (12), and then (11), and (6–8) to obtain $u_{\mathrm{bulk},B}$, $n_{\mathrm{bulk},B}$, $T_{\mathrm{bulk},B}$, $dT_{\mathrm{bulk},B}/dz$, and τ_{T_B}.

6) Use Eq. (4) to calculate x_B.

7) Use Eqs. (1–3) to calculate β_B^*, wall temperature T_B^*, and equilibrium vapor density $n_{\mathrm{eq},B}^*$.

8) If the calculated T_B^* and $n_{\mathrm{eq},B}^*$ are not equal to given wall temperature T_B and equilibrium number density $n_{\mathrm{eq},B}$, go to step 1 and change x_A and τ_{T_A}.

In this work, the Newton–Raphson method [24] was used to iterate over the values of x_A and τ_{T_A}. The mass of vapor molecules and gas thermal conductivity in the bulk region have been chosen as

$$\begin{aligned} m &= 7.7467 \cdot 10^{-27}\ \mathrm{kg} \quad \text{and} \\ \chi_{\mathrm{gas}} &= 0.10022 \cdot (T/273)^{3/4}\ \mathrm{W/(m \cdot K)} \end{aligned} \tag{18}$$

and the input parameters of the runs are shown in Table 1. Because there are two Knudsen layers (Fig. 1), the Knudsen numbers in Table 1 have been taken as $2 \cdot \lambda_{\mathrm{mfp}}/L$, where λ_{mfp} has been calculated using Eq. (7) for $T = 300$ K.

The region between the plates was divided into 10,000 uniform cells to numerically solve Eq. (15) and 10,000 iterations were used in the Newton–Raphson method to obtain x_A and τ_{T_A}. The code was

Table 1 Input parameters for modeling

L, m	T_A, K	$n_{\mathrm{eq},A}$, m^{-3}	T_B, K	$n_{\mathrm{eq},B}$, m^{-3}	λ_{mfp}. m	Kn
5.24×10^{-4}	300	4.59×10^{22}	413.24	3.06×10^{22}	1.31×10^{-4}	0.5
1.31×10^{-3}	300	4.59×10^{22}	413.24	3.06×10^{22}	1.31×10^{-4}	0.2
2.62×10^{-3}	300	4.59×10^{22}	413.24	3.06×10^{22}	1.31×10^{-4}	0.1
5.24×10^{-3}	300	4.59×10^{22}	413.24	3.06×10^{22}	1.31×10^{-4}	0.05
1.31×10^{-2}	300	4.59×10^{22}	413.24	3.06×10^{22}	1.31×10^{-4}	0.02
2.62×10^{-2}	300	4.59×10^{22}	413.24	3.06×10^{22}	1.31×10^{-4}	0.01

written in Java; each run took a few minutes on a PC with a Pentium 4 processor. Increasing the space steps by a factor of 2 (i.e., using 5×10^3 intervals) led to relative errors in x_A and τ_{T_A} of 7×10^{-6} and 3.5×10^{-4}, respectively, for $L = 2.62 \times 10^{-2}$ m; they monotonically decrease with L down to 7×10^{-7} for $L = 5.24 \times 10^{-4}$ m.

III. Kinetic Approaches

Two kinetic approaches have been used in this work for the verification of the Pekker–Keidar–Cambier analytical model [13] of the Knudsen layer: the DSMC method and the solution of the ES–BGK model kinetic equation.

In the DSMC calculations, the DSMC-based computational tool SMILE has been used (details on the tool may be found in [25]). The complete sticking of particles collided with the surface was assumed to model the condensation process. The evaporation process was modeled with the incoming particles entering the computational domain from the walls; their velocities were sampled from the equilibrium distribution function with the corresponding surface temperature. The one-dimensional problem shown in Fig. 1 was computed using the 2-D module of SMILE with a single row of cells bounded by specularly reflecting walls in the transversal direction and the longitudinal walls at A and B surfaces (Fig. 1) absorbing all incident particles. The majorant frequency scheme [26] was employed for modeling molecular collisions. The variable hard sphere model [27] was used for intermolecular interactions, with the reference particle diameter of 2.8 Å at a reference temperature of 273 K and the exponent in the viscosity-temperature dependence of 0.75. The DSMC modeling was conducted for $L = 5.24 \times 10^{-4}$ and 5.24×10^{-3} m, for which convergence of the grid and number of molecules was obtained. The results shown herein were obtained for a uniform spatial grid with 4000 cells and about 4 million molecules and ran over 1 million time steps that took approximately 300 computer processing hours (CPH). The numerical error is estimated to be about 1%.

The finite volume solver SMOKE, developed at ERC, Inc., was used to solve the ES–BGK equation. SMOKE is a parallel code based on a conservative numerical scheme developed by Mieussens [28]. A second-order spatial discretization was used along with implicit time integration. The boundary conditions at the A and B surfaces were set to simulate the condensation coefficient of unity, and the distribution function in the ghost cells was equilibrium with the corresponding parameters specified in Table 1. The viscosity-temperature dependence was the same as in the DSMC modeling. The spatial grid convergence was achieved by increasing the number of nodes from 200 to 2000 with nonuniform cell sizes to account for stronger gradients near the walls. The convergence on the velocity grid was also studied with the number of bins in the (x, y, z) directions ranging from (10, 10, 10) to (30, 20, 20). The longest run for $L = 2.62 \times 10^{-2}$ m (Table 1) took approximately 15 CPH. The numerical error is estimated to be less then 1.5%.

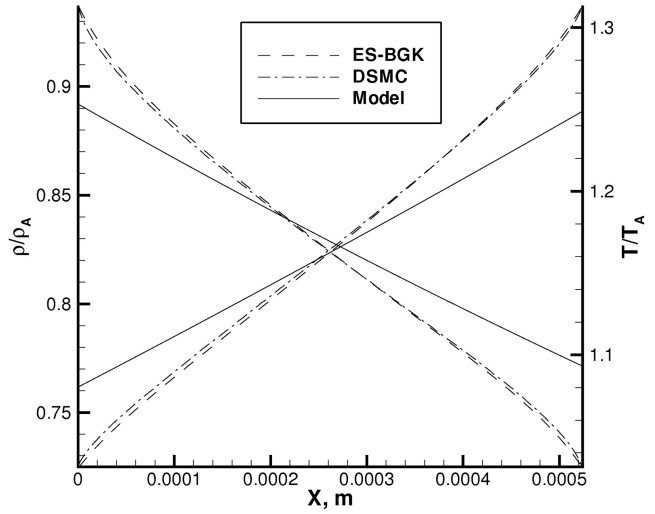

Fig. 3 Density and temperature between the ablative plates for two kinetic approaches and the analytic model for $L = 5.24 \times 10^{-4}$ m.

IV. Numerical Results and Analysis

Let us first compare the distributions of gas density and temperature obtained using the two kinetic approaches with those

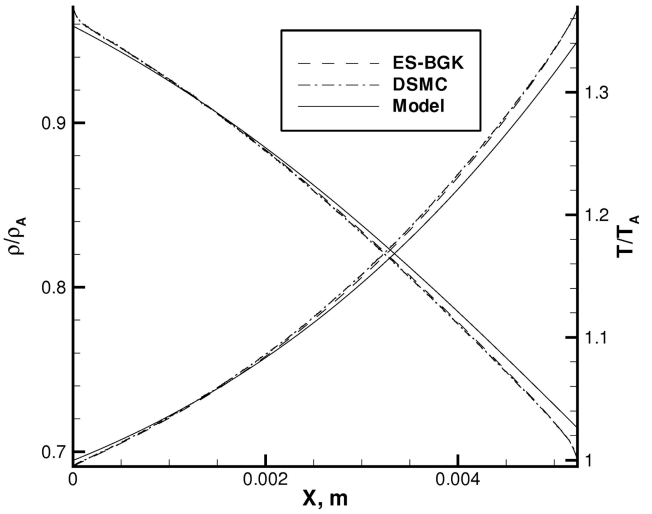

Fig. 4 Density and temperature between the ablative plates for two kinetic approaches and the analytic model for $L = 5.24 \times 10^{-3}$ m.

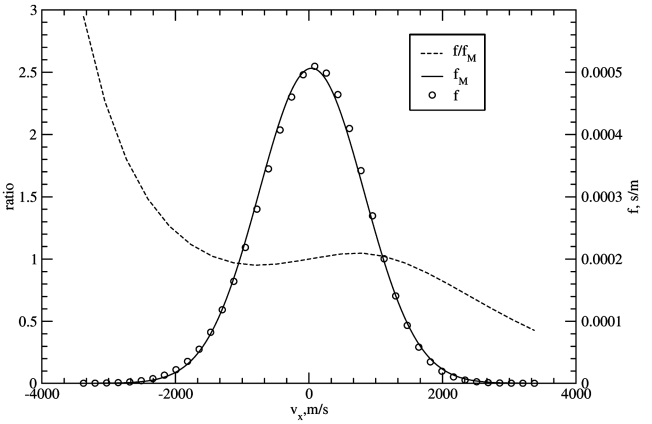

Fig. 5 Longitudinal velocity distribution functions in the center of the computational domain $L = 5.24 \times 10^{-4}$ m.

Table 2 Mass, energy, and momentum fluxes

		Analytical			ES–BGK			DSMC	
L, m	λ_{mnf}, m	M_x, $kg \cdot m^{-2} \cdot s^{-1}$	P_x, $kg \cdot m^{-2} \cdot s^{-2}$	E_x, $W \cdot m^{-2}$	M_x, $kg \cdot m^{-2} \cdot s^{-1}$	P_x, $kg \cdot m^{-2} \cdot s^{-2}$	E_x, $W \cdot m^{-2}$	M_x, $kg \cdot m^{-2} \cdot s^{-1}$	E_x, $W \cdot m^{-2}$
5.24×10^{-4}	1.31×10^{-4}	1.043×10^{-2}	182.52	4585	1.193×10^{-2}	182.53	2836	1.178×10^{-2}	2638
1.31×10^{-3}	1.31×10^{-4}	8.910×10^{-3}	182.45	6755	9.475×10^{-3}	182.46	6280	——	——
2.62×10^{-3}	1.31×10^{-4}	7.994×10^{-3}	182.38	8060	8.249×10^{-3}	182.40	7978	——	——
5.24×10^{-3}	1.31×10^{-4}	7.412×10^{-3}	182.34	8887	7.553×10^{-3}	182.34	8955	7.380×10^{-3}	8832
1.31×10^{-2}	1.31×10^{-4}	7.106×10^{-3}	182.31	9322	7.198×10^{-3}	182.32	9433	——	——
2.62×10^{-2}	1.31×10^{-4}	7.075×10^{-3}	182.31	9366	7.169×10^{-3}	182.31	9485	——	——

Table 3 Relative differences between the analytical, ES–BGK, and DSMC results

L, m	λ_{mfp}, m	Kn	$\hat{M}_{x,analyt}$, %	$\hat{E}_{x,analyt}$, %	$\hat{M}_{x,DSMC}$, %	$\hat{E}_{x,DSMC}$, %
5.24×10^{-4}	1.31×10^{-4}	0.5	12.55	−61.65	1.25	6.99
1.31×10^{-3}	1.31×10^{-4}	0.2	5.96	−7.56	——	——
2.62×10^{-3}	1.31×10^{-4}	0.1	3.09	−1.02	——	——
5.24×10^{-3}	1.31×10^{-4}	0.05	1.87	0.76	2.29	2.49
1.31×10^{-2}	1.31×10^{-4}	0.02	1.28	1.17	——	——
2.62×10^{-2}	1.31×10^{-4}	0.01	1.31	1.26	——	——

obtained with the analytical model. The results for the most rarefied case, $L = 5.24 \times 10^{-4}$ m and $Kn = 0.5$, are presented in Fig. 3.

As one can see, there is a reasonable agreement between the DSMC and ES–BGK solutions, with the exception of the region close to the wall. However, the density and temperature distributions obtained by the analytical approach are far off from the kinetic distributions. This observation has a simple explanation. In all analytical models of the Knudsen layer [1–14], the Knudsen layer is considered as a zero-dimensional interface between the wall and gas bulk. However, in this situation, in which the summarized thickness of the two Knudsen layers is only 2 times smaller than the gap between the walls (Fig. 1), this approximation is not valid.

The difference between the kinetic and analytical distributions of gas macroparameters becomes smaller as the Knudsen number decreases, as illustrated in Fig. 4, in which $L = 5.24 \times 10^{-3}$ m and $Kn = 0.05$ (Table 1). It is clear that this difference is much smaller than for the case of $L = 5.24 \times 10^{-4}$, but still noticeable. This, again, can be explained by neglecting the thickness of the Knudsen layer in the analytical model [13].

The effect of thermal nonequilibrium in the ES–BGK solution is illustrated in Fig. 5, in which the computed distribution function of the longitudinal velocity is compared with the corresponding Maxwellian distribution function with the local temperature and velocity for $L = 5.24 \times 10^{-4}$ at $x = L/2$. The ratio of the ES–BGK solution to the Maxwellian distribution is also shown in Fig. 5. In the central region [the velocity is close to the averaged longitudinal velocity, u_{bulk}, in Eq. (9)], the deviation of the computed function from the Maxwellian distribution is relatively small, whereas for the tails of the distribution functions it reaches a factor of 2 and more.

The most important properties that the analytical model is expected to provide are the mass, momentum, and energy fluxes from the cold to the hot ablative surfaces. A comparison of fluxes computed using different approaches is given in Table 2. With an increase in the distance between the plates, the mass fluxes decrease while the energy fluxes increase for all three models. With an increase in L and fixed T_A and T_B, the thermal conduction heat flux to surface A decreases; therefore, M_x (the evaporation rate from plate A) decreases too. Because, with an increase in L, the energy flux directed from the cold surface to the hot surface [the second term on the right-hand side of Eq. (11)] decreases faster than the thermal conduction (the first term), E_x increases with an increase in L, as shown in Table 2. However, with further increases in L, at some point, when the gap between the plates becomes too large, E_x has to reach its maximum and then will decrease down to zero, when $L \to \infty$. The momentum flux materially does not change with the distance between the plates, because it is related mostly to the gas bulk pressure, Eq. (10), which in turn is determined by the outflow conditions at the plates (equilibrium vapor pressures) and not by the distance between the plates.

The relative differences between the ES–BGK solution and either the analytical and DSMC results are calculated with the following formula:

$$\hat{M}_{x,\alpha} = 100 \cdot \frac{(M_{x,\mathrm{BGK}} - M_{x,\alpha})}{M_{x,\mathrm{ES-BGK}}}, \quad \hat{E}_{x,\alpha} = 100 \cdot \frac{(E_{x,\mathrm{BGK}} - E_{x,\alpha})}{E_{x,\mathrm{ES-BGK}}} \tag{19}$$

where index α denotes either the analytical or DSMC solution. Table 3 shows the relative differences between the ES–BGK solution and either the analytical and DSMC results that were calculated with the following formula: $L \geq 5.24 \cdot 10^{-3}$. For the smaller L (larger Knudsen numbers), there is a noticeable difference between the kinetic solutions and analytical approach. The differences in the energy fluxes $\hat{E}_{x,DSMC}$ and $\hat{E}_{x,analyt}$ reach about 7 and 61%, respectively, for $L = 5.24 \times 10^{-4}$. Such differences are expected because the ES–BGK model is a simplification of the Boltzmann equation, whereas the analytical approximation assumes a small deviation from the Maxwellian distribution function (small Knudsen numbers). The ES–BGK model works better for relatively large Knudsen numbers than the analytical approximation (Table 3). However, for $L = 1.31 \times 10^{-3}$, the differences in mass and energy fluxes obtained by the ES–BGK and analytical approaches are about 6 and −7.6%, respectively.

Thus, one may conclude that the numerical results clearly show that the Pekker–Keidar–Cambier analytical model [13] of the Knudsen layer provides reasonable estimates for the mass, energy, and momentum fluxes for Knudsen numbers less than 0.2.

V. Conclusions

One of the most important issues in CFD modeling of ablation processes is the specification of the boundary conditions at the gas–surface interface. These boundary conditions cannot be obtained without analytical or parametric numerical modeling of the Knudsen layer formed near the evaporating surface. The main objective of the present paper was to provide a detailed analysis of the applicability of a recently developed analytical model of the Knudsen layer [13] by comparing its predictions with the ES–BGK and DSMC results. To verify this model, a one-dimensional evaporation/condensation process between two parallel plates was considered for different Knudsen numbers.

The analytical approach that incorporates the model of the Knudsen layer [13] was found to capture well the mass, energy, and

momentum fluxes across the Knudsen layer for Knudsen numbers less than 0.2. Thus, one may conclude that the gas–surface boundary conditions obtained in [13] can be used fairly successfully in CFD modeling of ablative processes when a Knudsen number is less than 0.2.

It has been demonstrated that for relatively large Knudsen numbers the ES–BGK model works better than the analytical approximation. For a Knudsen number of 0.5, the difference in the mass and energy fluxes obtained by the ES–BGK and DSMC solutions is about 1.3 and 7%, respectively.

References

[1] Hertz, H., "Over the Evaporation of the Fluids, Especially the Mercury, in the Air Empty Room," *Annalen der Physik (Leipzig)*, Vol. 253, No. 10, 1882, pp. 177–193. doi:10.1002/andp.18822531002

[2] Knudsen, M., "The Maximum Evaporation Speed of the Mercury," *Annalen der Physik (Leipzig)*, Vol. 352, No. 13, 1915, pp. 697–708. doi:10.1002/andp.19153521306

[3] Park, C., *Nonequilibrium Hypersonic Aerothermodynamics*, Wiley-Interscience, Canada, 1990.

[4] Ahn, H.-K., Park, C., and Sawada, K., "Dynamics of Pyrolysis in Charring Materials Ablation," AIAA Paper 98-0165, Jan. 1998.

[5] Bond, M., and Struchtrup, H., "Mean Evaporation and Condensation Coefficients Based on Energy Dependent Condensation Probability," *Physical Review E (Statistical Physics, Plasmas, Fluids, and Related Interdisciplinary Topics)*, Vol. 70, No. 6, 2004, pp. 061–605. doi:10.1103/PhysRevE.70.061605

[6] Anisimov, S. I., "Vaporization of Metal Absorbing Laser Radiation," *Soviet Physics Journal of Experimental and Theoretical Physics*, Vol. 27, No. 1, 1968, pp. 182–183.

[7] Ytrehus, T., "Theory and Experiments on Gas Kinetics in Evaporation," *Rarefied Gas Dynamics*, Vol. 51, AIAA, New York, 1976, pp. 1197–1213.

[8] Beilis, I. I., "Parameters of the Knudsen Layer of Arc-Discharge Cathode Region," *IEEE Transactions on Plasma Science*, Vol. 13, No. 5, 1985, pp. 288–290. doi:10.1109/TPS.1985.4316422

[9] Beilis, I. I., "Theoretical Modeling of Cathode Spot Phenomena," *Vacuum Arc Science and Technology*, edited by R. L. Boxman, P. Martin, D. Sanders, Noyes Publications, Park Ridge, NJ, 1995.

[10] Keidar, M., Fan, J., Boyd, I. D., and Beilis, I. I., "Vaporization of Heated Materials into Discharge Plasmas," *Journal of Applied Physics*, Vol. 89, No. 6, 2001, pp. 3095–3098. doi:10.1063/1.1345860

[11] Keidar, M., Boyd, I. D., and Beilis, I. I., "On the Model of Teflon Ablation in an Ablation-Controlled Discharge," *Journal of Physics D: Applied Physics*, Vol. 34, No. 11, 2001, pp. 1675–1677. doi:10.1088/0022-3727/34/11/318

[12] Keidar, M., Boyd, I. D., and Beilis, I. I., "Ionization and Ablation Phenomena in an Ablative Plasma Accelerator," *Journal of Applied Physics*, Vol. 96, No. 10, 2004, pp. 5420–5428. doi:10.1063/1.1805726

[13] Pekker, L., Keidar, M., and Cambier, J.-L., "Effect of Thermal Conductivity on the Knudsen Layer at Ablative Surfaces," *Journal of Applied Physics*, Vol. 103, 2008, pp. 034–906. doi:10.1063/1.2838210

[14] Pekker, L., "An Analytical Model of Ablation Using a Bimodal Velocity Distribution Function in the Knudsen Layer," AIAA Paper 2008-3910, June 2008.

[15] Bird, G. A., *Molecular Gas Dynamics and the Direct Simulation of Gas Flow*, Clarendon, Oxford, 1994.

[16] Sibold, D., and Urbassek, H. M., "Kinetic Study of Pulsed Desorption Flows into Vacuum," *Physical Review A*, Vol. 43, No. 12, 1991, pp. 6722–6734. doi:10.1103/PhysRevA.43.6722

[17] Sibold, D., and Urbassek, H. M., "Monte Carlo Study of the Knudsen Layers in Evaporation from Elemental and Binary Media," *Physics of Fluids A*, Vol. 5, No. 1, 1993, pp. 243–256. doi:10.1063/1.858779

[18] Morozov, A. A., "Thermal Model of Pulsed Laser: Back Flux Contribution," *Applied Physics A: Materials Science and Processing*, Vol. 79, Nos. 4–6, 2004, pp. 997–999. doi:10.1007/s00339-004-2613-2

[19] Bhatnagar, P. L., Gross, E. P., and Krook, M. A., "A Model for Collision Processes in Gases. I. Small Amplitude Processes in Charged and Neutral One-Component Systems," *Physical Review*, Vol. 94, No. 3, 1954, pp. 511–525. doi:10.1103/PhysRev.94.511

[20] Holway, L. H., "Kinetic Theory of Shock Structure Using an Ellipsoidal Distribution Function," *Proceedings of the Fourth International Symposium on Rarefied Gas Dynamics*, Academic Press, New York, 1966, pp. 193–215.

[21] Shishkova, I. N., and Sazhin, S. S., "A Numerical Algorithm for Kinetic Modeling of Evaporation Processes," *Journal of Computational Physics*, Vol. 218, No. 2, 2006, pp. 635–653. doi:10.1016/j.jcp.2006.02.019

[22] Rose, J. W., "Accurate Approximation Equations for Intensive Sub-Sonic Evaporation," *International Journal of Heat and Mass Transfer*, Vol. 43, No 20, 2000, pp. 3869–3875. doi:10.1016/S0017-9310(00)00018-1

[23] Vincenti, W. G., and Kruger, C. H., Jr., *Introduction to Physical Gas Dynamics*, Krieger, Malabar, FL, 1975.

[24] Press, W. H., Teukolsky, S. A., Vetterling, W. T., and Flannery, B. P., *Numerical Recipes: The Art of Scientific Computing*, 3rd ed., Cambridge Univ. Press, New York, 2007.

[25] Ivanov, M. S., Markelov, G. N., and Gimelshein, S. F., "Statistical Simulation of Reactive Flows: Numerical Approach and Applications," AIAA Paper 1998-2669, 1998.

[26] Ivanov, M. S., and Rogasinsky, S. V., "Analysis of Numerical Techniques of the Direct Simulation Monte Carlo Method in the Rarefied Gas Dynamics," *Soviet Journal of Numerical Analysis and Mathematical Modeling*, Vol. 2, No. 6, 1988, pp. 453–465.

[27] Bird, G. A., "Monte Carlo Simulation in an Engineering Context," *Rarefied Gas Dynamics*, edited by S. Fisher, Part 1, AIAA, New York, 1981, pp. 239–255.

[28] Mieussens, L., "Discrete-Velocity Models and Numerical Schemes for the Boltzmann-BGK Equation in Plane and Axisymmetric Geometries," *Journal of Computational Physics*, Vol. 162, No. 2, 2000, pp. 429–466. doi:10.1006/jcph.2000.6548